Geophysical Research Letters

RESEARCH LETTER
10.1029/2021GL095509

Impact of the Juan Fernandez Ridge on the Pampean Flat Subduction Inferred From Full Waveform Inversion

Yajian Gao[1,2], Xiaohui Yuan[1], Benjamin Heit[1], Frederik Tilmann[1,2], Dirk-Philip van Herwaarden[3], Solvi Thrastarson[3], Andreas Fichtner[3], and Bernd Schurr[1]

[1]GFZ German Research Centre for Geosciences, Potsdam, Germany, [2]Freie Universität Berlin, Berlin, Germany, [3]ETH Zürich, Zürich, Switzerland

Key Points:

- A new seismic model for the crust and upper mantle beneath central Chile and western Argentina is presented
- Thinning and tearing within the Pampean flat slab is detected along the inland projection of the Juan Fernandez Ridge
- A relic slab is imaged beneath the Pampean flat slab, reflecting slab break-off during the flattening process

Supporting Information:

Supporting Information may be found in the online version of this article.

Correspondence to:

Y. Gao,
yjgao@gfz-potsdam.de

Citation:

Gao, Y., Yuan, X., Heit, B., Tilmann, F., van Herwaarden, D.-P., Thrastarson, S., et al. (2021). Impact of the Juan Fernandez Ridge on the Pampean flat subduction inferred from full waveform inversion. *Geophysical Research Letters*, *48*, e2021GL095509. https://doi.org/10.1029/2021GL095509

Received 4 AUG 2021
Accepted 9 OCT 2021

Abstract A new seismic model for crust and upper mantle of the south Central Andes is derived from full waveform inversion, covering the Pampean flat subduction and adjacent Payenia steep subduction segments. Focused crustal low-velocity anomalies indicate partial melts in the Payenia segment along the volcanic arc, whereas weaker low-velocity anomalies covering a wide zone in the Pampean segment are interpreted as remnant partial melts. Thinning and tearing of the flat Nazca slab is inferred from gaps in the slab along the inland projection of the Juan Fernandez Ridge. A high-velocity anomaly in the mantle below the flat slab is interpreted as relic Nazca slab segment, which indicates an earlier slab break-off triggered by the buoyancy of the Juan Fernandez Ridge during the flattening process. In Payenia, large-scale low-velocity anomalies atop and below the re-steepened Nazca slab are associated with the re-opening of the mantle wedge and sub-slab asthenospheric flow, respectively.

Plain Language Summary Taking advantage of the abundant information recorded in seismic waveforms, we imaged the seismic structure of the crust and upper mantle beneath central Chile and western Argentina, where the oceanic Nazca slab is subducting beneath the South American plate. The subducted Nazca slab is almost flat at a depth of 100–150 km in the north of the study area below the Pampean region, where the Juan Fernandez seamount ridge is subducting as part of the Nazca slab. The slab steepens again in the south in the Payenia region. Our model reveals pronounced low-velocity anomalies within the Pampean flat slab along the inland projection of the Juan Fernandez Ridge, indicating that the Pampean flat slab is thinned or even torn apart. A high-velocity anomaly is imaged beneath the flat slab, representing a former slab segment that was broken off during the slab flattening process and was overridden by the advancing young slab. Our model suggests a causal relationship between the oceanic ridge subduction and the flat slab formation. In the Payenia region, the slab re-steepening resulted in the re-establishment of the mantle wedge and induced hot mantle flow below the slab, which are characterized by low-velocity anomalies in the model.

1. Introduction

The temporal and spatial appearances of flat subduction segments along the South American western margin have been extensively debated (e.g., Antonijevic et al., 2015; Gutscher et al., 2000; Marot et al., 2014; Ramos & Folguera, 2009). Two prominent flat subduction segments beneath the Andes are the Peruvian and Pampean flat subduction zones, north and south of the conspicuous kink in the South American coastline, respectively. They have been documented based on seismology (e.g., Pesicek et al., 2012; Wagner et al., 2005), volcanism (e.g., Kay & Abbruzzi, 1996; Kay & Mpodozis, 2002), gravity modeling (e.g., Sánchez et al., 2019) and electrical conductivity measurements (e.g., Burd et al., 2013, 2014). In this study, we focus on the Pampean flat subduction and Payenia steep subduction to the south, from 28°–38°S (Figure 1). Here, the Nazca slab is subducting beneath central Chile and western Argentina with a convergence rate of ~6.7 cm a^{-1} in the N78°E direction (Kendrick et al., 2003). In the Pampean flat subduction zone (Kay & Mpodozis, 2002; Ramos et al., 2002), the Nazca slab propagates horizontally for 200–300 km beneath the southern Central Andes (Figure 1a) whereas the Payenia segment was dominated by flat subduction period from 15 to 5 Ma but has been re-steepening since 4–5 Ma (Ramos & Folguera, 2009, 2011).

The current Pampean flat subduction zone is widely believed to be associated with the subduction of the Juan Fernandez seamount ridge (JFR, Figure 1; e.g., Gutscher et al., 2000; Kay & Mpodozis, 2002; Ramos

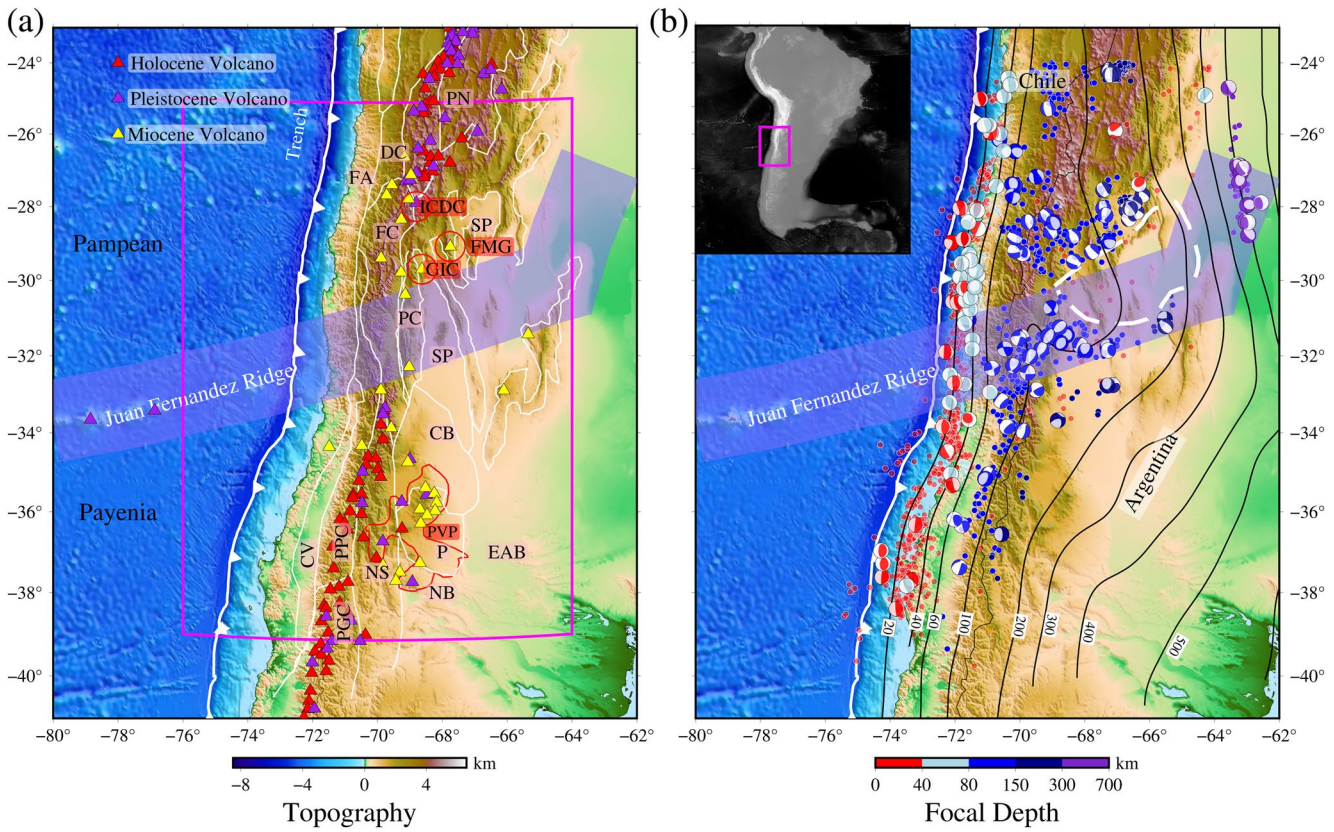

Figure 1. Tectonic setting of the South Central Andes, with the Nazca plate subducting to the east beneath the South America plate. (a) Major morphotectonic provinces are modified from Tassara et al. (2006) and Piceda et al. (2020), including Fore-Arc (FA), Domeyko Cordillera (DC), Frontal Cordillera (FC), Puna (PN), Precordillera (PC), Subandean Ranges (SA), SierrasPampeanas (SP), Patagonian Cordillera (PGC), Principal Cordillera (PPC), Central Valley (CV), Neuquen Basin (NB), Neuquen System (NS), Payenia Craton (P), Payenia Volcanic Province (PVP), Incapillo Caldera and Dome Complex (ICDC), Famatina Mogotes Group (FMG), Gualcamayo Igneous Complex (GIC). The solid red line denotes the Payenia Volcanic Province (Ramos & Folguera, 2011). White saw-tooth line denotes the trench. (b) Map showing focal mechanisms of the earthquakes used for FWI. Color-coded dots represent the seismicity (magnitude > Mw 4.0) retrieved from the ISC-EHB catalog (Engdahl et al., 2020). Solid black lines are the Nazca slab contours from Slab 2.0 (Hayes et al., 2018). The thick dashed white line denotes the intraslab aseismic zone. Topography data is retrieved from ETOPO1 Global Relief Model (Amante & Eakins, 2009). Inset map marks the position of our study region.

et al., 2002). Plate reconstructions (Bello-González et al., 2018; Yáñez et al., 2001) indicate that the ridge has been moving southward along the western margin of South America. It was subducting beneath the Altiplano and Puna plateaus (20°–26°S) at ~40–20 Ma, inducing temporary flat subduction and inland migration of volcanism and a temporary lull between 20 and 12 Ma (Beck et al., 2015; Kay & Coira, 2009; Yáñez et al., 2001). The JFR arrived at the current position beneath the Sierras Pampeanas around 12 Ma (Figure 1) and the related flat subduction of the Nazca slab has again triggered inland migration and cessation of the subduction-related volcanism (Kay & Mpodozis, 2002), uplift of the main Andes, thick-skinned deformation, crustal thickening and basement uplift over a broad zone in the overriding plate (Cristallini & Ramos, 2000; Ramos et al., 2002). However, the mechanisms and consequences of the flat subduction are still under debate (Hu & Liu, 2016; Liu & Currie, 2019; Manea et al., 2012). In contrast, the sudden re-steepening of the Nazca plate beneath the Payenia segment is associated with the roll-back of the trench (Ramos et al., 2014); thus, the Payenia segment has undergone a complete cycle from crustal thickening, mountain uplift and inland migration of volcanism (Kay et al., 2005; Ramos & Folguera, 2009) during flat subduction to extensional collapse and trenchward migration of volcanism during the re-steepening period (5 Ma to now; Folguera et al., 2008; Ramos & Folguera, 2009; Ramos et al., 2014).

The geological timing of the slab angle variations is constrained by the deformation (e.g., Ramos & Folguera, 2009) and volcanism (e.g., Kay & Kay, 2002; Spagnuolo et al., 2012) history in both areas. However, existing seismic images still give an incomplete picture. Teleseismic tomography provides a good larger-scale

view of the upper mantle but has low vertical resolution, particularly at shallow depths, making it hard to distinguish velocity variations in the crust and uppermost mantle, while local travel time tomography studies can give insight into local structures and processes, for example, magma pathways feeding individual volcanic systems, but usually fail to image the full width of the subducting slab due to their small study scale; the small scale also hampers an understanding of the regional variations. Here, we employ seismic full waveform inversion (FWI) to better constrain the seismic structure in the crust and upper mantle beneath the south Central Andes, which would facilitate to further investigate the slab configuration and the crustal melt distributions in response to the subduction of the JFR in the Pampean and the mantle wedge evolution in response to the slab re-steepening in the Payenia

2. Data and Method

Following the same workflow as Gao et al. (2021), we collected 139 earthquakes from the Global Centroid-Moment-Tensor (GCMT) catalog (Ekström et al., 2012), which were recorded by 19 seismic networks (Figure 1 and Figure S1 in Supporting Information S1) operating between 1996 and 2019 and magnitudes between M_W 5.0 and 7.0. Detailed network information and raypath coverage are presented in Figures S1 - S2 and Table S1 in Supporting Information S1. Our seismic velocity model is the result of the multi-scale FWI based on the adjoint methodology (e.g., Fichtner et al., 2010; Tape et al., 2010) and started from the initial 3D V_P and V_S model *SP12RTS* (Koelemeijer et al., 2015). Solutions of the visco-elastic wave equation in a radially anisotropic Earth model are obtained from *Salvus* (Afanasiev et al., 2019). The inversion starts by inverting periods 60–120 s using a time-frequency phase shift misfit and proceeds progressively to shorter periods, with waveforms between 12 and 100 s being inverted for in the final iterations, using a cross-correlation coefficient based misfit function. More information about the inversion workflow is provided in Text S1, Figure S4, and Table S2 in Supporting Information S1.

To analyze the resolution of the inversion and trade-offs between the parameters, we calculated the Hessian-vector product Hδm as point-spread functions to assess possible smearing and distortion (Fichtner & Trampert, 2011; Tao et al., 2018). We find that the isotropic V_S and V_P models are robustly determined in the resolved region with a spatial resolution of 30–40 km in the upper mantle and 25–30 km in the crust, both horizontally and vertically. Detailed resolution tests are described in Text S2 and Figures S22–S32 in Supporting Information S1.

3. Results and Discussion

After 53 iterations of FWI, the crust and upper mantle structure beneath central Chile and western Argentina has been clearly imaged. We display the isotropic V_S model with some key depth and cross-sections. Further images and the isotropic V_P model are shown in Figures S5–S20 in Supporting Information S1.

3.1. Multi-Stage Crustal Partial Melting and Mantle Wedge Evolution

In contrast to the vigorous partial melting represented by strong low-velocity anomalies in the middle-crust beneath the Altiplano-Puna Volcanic Complex and volcanic arc for the northern Chile steep subduction zone (Gao et al., 2021; Ward et al., 2014; Yuan et al., 2000), the middle crust in the Pampean flat subduction zone (28°–33°S) exhibits only moderately low to normal velocities along the volcanic arc (Figure 2a).

Low-velocity anomaly C1 (Figure 2a and Figure S21 in Supporting Information S1) is located beneath the Frontal Cordillera (FC) and has been reported by several earlier studies (e.g., Gao et al., 2021; Ward et al., 2013, 2017). In agreement with these earlier studies, we interpret C1 to mark the waning partial melting (Gao et al., 2021; Ward et al., 2017) beneath the Incapillo Caldera and Dome Complex (ICDC, Figure 1a), which is the southernmost ignimbrite caldera of the Central Andes during the Pleistocene (Goss et al., 2009, 2011). Meanwhile, weak and isolated low-velocity anomalies (C2 and C3, Figure 2a) beneath the Sierras Pampeanas (SP) are accompanied by middle to late Miocene adakitic volcanoes including the Famatina Mogotes Group (FMG, Kay & Mpodozis, 2002) and Gualcamayo Igneous Complex (GIC, D'Annunzio

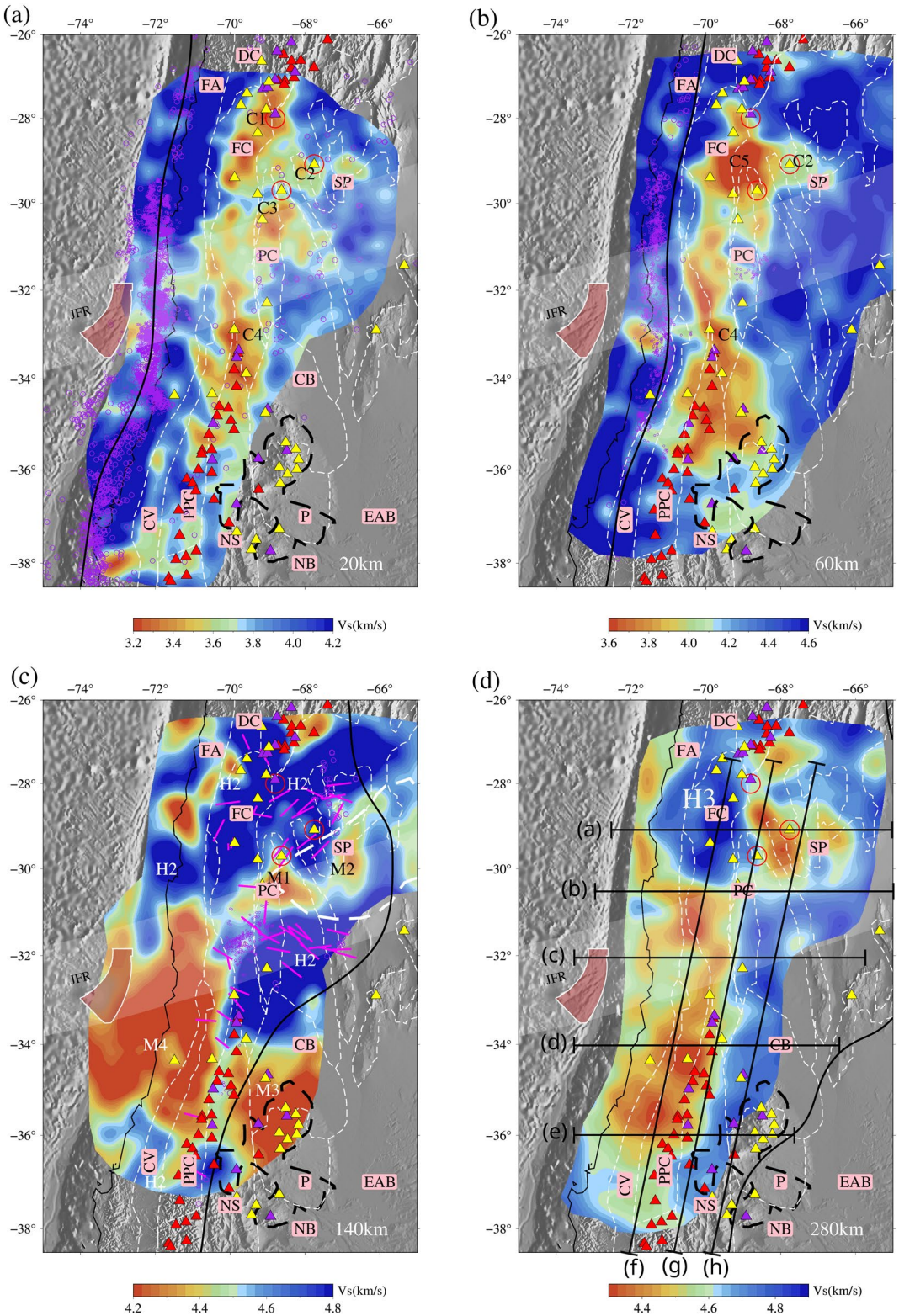
(a)
(b)
(c)
(d)
DC
FA
C1
FC
C2
SP
C3
PC
JFR
C4
CB
CV
PPC
P
EAB
NS
NB
20km
60km
140km
280km
C5
H2
M1
M2
M3
M4
H3
(e)
(f)
(g)
(h)
Vs(km/s)
3.2 3.4 3.6 3.8 4.0 4.2
3.6 3.8 4.0 4.2 4.4 4.6
4.2 4.4 4.6 4.8
4.4 4.6 4.8

Figure 2.

et al., 2018), hinting at the relic and waning slab melting origin (Gutscher et al., 2000; Hu & Liu, 2016; Kay & Abbruzzi, 1996; Kay & Kay, 2002) during the flattening process around 6–3 Ma (Hu & Liu, 2016).

A striking low-velocity anomaly C5 (Figure 2b and Profile [a] in Figure 3) at approximate Moho depth (60 km) extends from the Frontal Cordillera to the Sierras Pampeanas (SP), forming a thin layer above the Pampean flat slab. As the mantle wedge must have been thinned to a sliver or completely closed during the flattening of the Nazca slab (Gutscher et al., 2000; Manea et al., 2017), this low-velocity anomaly could be attributed to the hydrated continental lithosphere due to the accumulation of fluids released from the current flat slab (Hildreth & Moorbath, 1988). The flat slab has the potential to significantly modify the overriding lithosphere for a long distance from the trench due to the dehydration (Hiett et al., 2021; Li, 2020; Marot et al., 2014) or scraping-off of the base of the continental mantle lithosphere, as has been suggested for the Laramide orogeny (Axen et al., 2018) and the North China Craton (Li, 2020) from numerical modeling.

In contrast, south of 33°S, C4 may mark the restoration of partial melt accumulation in the middle crust during the re-steepening process of the Nazca slab beneath the Payenia (Marot et al., 2014; Ramos & Folguera, 2009). The late Miocene volcanic activity in the back-arc and Pleistocene-Holocene volcanic activity in the frontal arc (including large-scale Payenia Volcanic Province, Figure 1a) indicate a trench-ward migration of the volcanism. Following the re-steepening of the slab since 4–5 Ma, the mantle wedge has re-opened, leading to the re-injection of hot asthenosphere and renewed melt formation in the wedge induced by slab-derived fluids dehydration, in turn inducing trench-ward migration of the volcanism (Gutscher et al., 2000; Kay & Mpodozis, 2002; Marot et al., 2014; Ramos & Folguera, 2009, 2011). The re-opened mantle wedge is clearly imaged in our model as low-velocity anomaly M3 and represents the present situation after the slab re-steepening (Figure 2c and profile [d] and [e] in Figure 3).

3.2. Slab Thinning and Tearing Along the Juan Fernandez Ridge

In the central part of the Pampean flat slab, two low-velocity anomalies (M1 and M2) span a slab window along the inland projection of the JFR (Figure 2c and Profile [b] in Figure 3) and are surrounded by two high-velocity limbs of the flat slab (H2). Though many prior works detected the Pampean flat slab with strong heterogeneities, most of seismological studies focused on the seismic structure south of 29°S (e.g., Linkimer et al., 2020; Marot et al., 2014; Porter et al., 2012; Wagner et al., 2005), leaving an observational gap from 27°–29°S. In this study, events and stations north of 27°S are included in the inversion, allowing us to resolve M1 and M2.

The inland projection of the JFR is not well constrained from previous plate reconstruction studies (Bello-González et al., 2018; Yáñez et al., 2001) due to its relatively long subduction and migration history (12 Ma) beneath the Pampean area. Hence, the extent of the region affected by the JFR is not known precisely, nor are details of the seismic structure associated with the JFR (Gans et al., 2011; Gutscher et al., 2000; Haddon & Porter, 2018; Marot et al., 2014; Wagner et al., 2005). Following Kay and Mpodozis (2002), we assume the uncertainty width of the influence zone of the JFR within the oceanic lithosphere is 200 km, which also takes into account the region of underplating and possible hydration of the oceanic lithosphere (Kopp et al., 2004), which extends beyond the seamount chain itself. Thus, the low-velocity anomalies M1 and M2 are located within the JFR influence range. Similar to predictions from numerical modeling (Hu & Liu, 2016), the slab thinning and tearing zone develops within the central part of the current flat slab. In Hu and Liu's model, slab thinning and tearing initiates from the inboard tip of the flat slab before re-steepening downdip and propagates trench-wards, parallel to the track of the JFR and consistent our direct observation. In addition to the enhanced buoyancy of the JFR, its hydration state and inherited normal faults (Kopp et al., 2004) might have caused zones of weakness along which the thinning and tearing could progress.

Figure 2. Horizontal depth slices for isotropic V_S. The large and small magenta circles are seismicity from ISC-EHB catalog and the relocated catalog from Sippl et al. (2021), respectively, within 10 km of the nominal depth of the slice. The off-shore pink-shaded area indicates the position of the weakened oceanic lithosphere detected by Kopp et al. (2004) along the Juan Fernandez seamount ridge. The solid black lines denote the top interface of the slab according to Slab 2.0 (Hayes et al., 2018) at the depth of the slice. Thick dashed black line denotes the Payenia Volcanic Province. In panel (c) T (tension) axes from Global Centroid-Moment-Tensor focal mechanism solutions (Ekström et al., 2012) for earthquakes between 120 and 150 km depth with magnitude M_W >5.0 are indicated by magenta bars. Straight black lines in panel (d) denote the positions of the cross-sections in Figure 3.

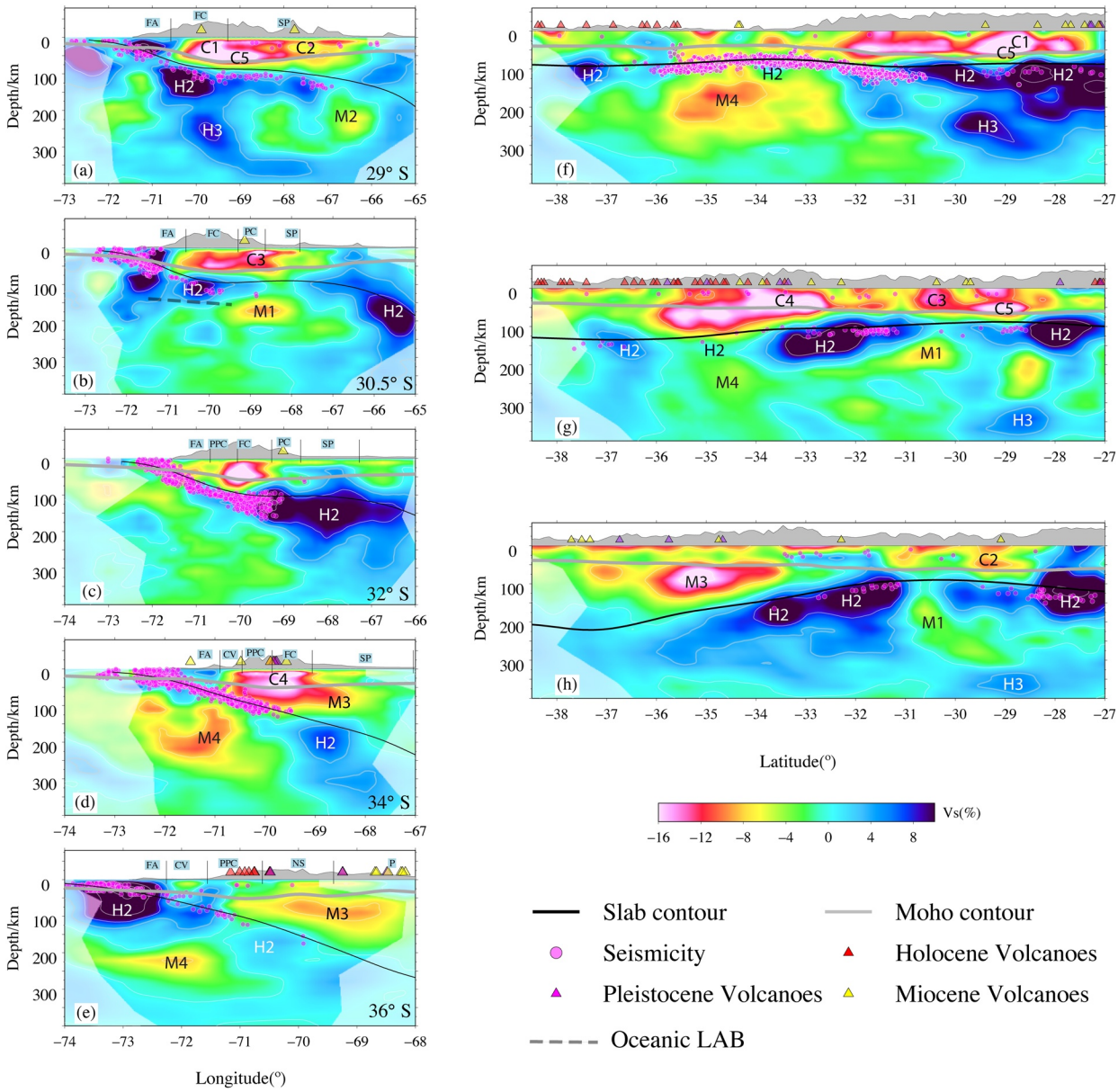

Figure 3. Cross-sections of isotropic V_S perturbations relative to the reference 1D V_S defined in Figure S3 in Supporting Information S1. (see Figure 2d for profile locations). The thick solid gray lines denote the continental Moho (Rivadeneyra-Vera et al., 2019) and thin solid black lines denote the slab contour from Slab 2.0 (Hayes et al., 2018). The thick dashed dark-gray line in panel (b) denotes the oceanic LAB from receiver function (Heit et al., 2008). Magenta dots in panels (b)–(d) denote the seismicity relocated by Sippl et al. (2021) and in other profiles are retrieved from ISC-EHB catalog. All the labeled tomographic anomalies can be found in the main text. See Figure S14 in Supporting Information S1 for a version of this figure without labels and seismicity.

Conspicuously, the slab tearing zone (M1 and M2) is characterized by the absence of intra-slab seismicity, in contrast to the slab limbs to the north and south (Figure 2c). The focal mechanisms show a clear asymmetric pattern across the JFR track: The north branch of H2 is characterized by predominantly NE-SW oriented T axes, which are subparallel to the track of the JFR, whereas the T axes for events in the southern branch of H2 are oriented mainly NW-SE, sub-normal to the JFR trend, implying a ~ 90° rotation of T axes across the aseismic zone (Figure 2c) at 120–160 km at depth. The northeast extension in the northern slab limb parallel to the JFR is superimposed on dominant slab pull (downdip extension), which is also reflected in the velocity field (Hu & Liu, 2016) and azimuthal anisotropy (Hu et al., 2017; Lynner et al., 2017). The south branch is coincident with the track of the JFR and attributed to the reactivation of the preexisting normal

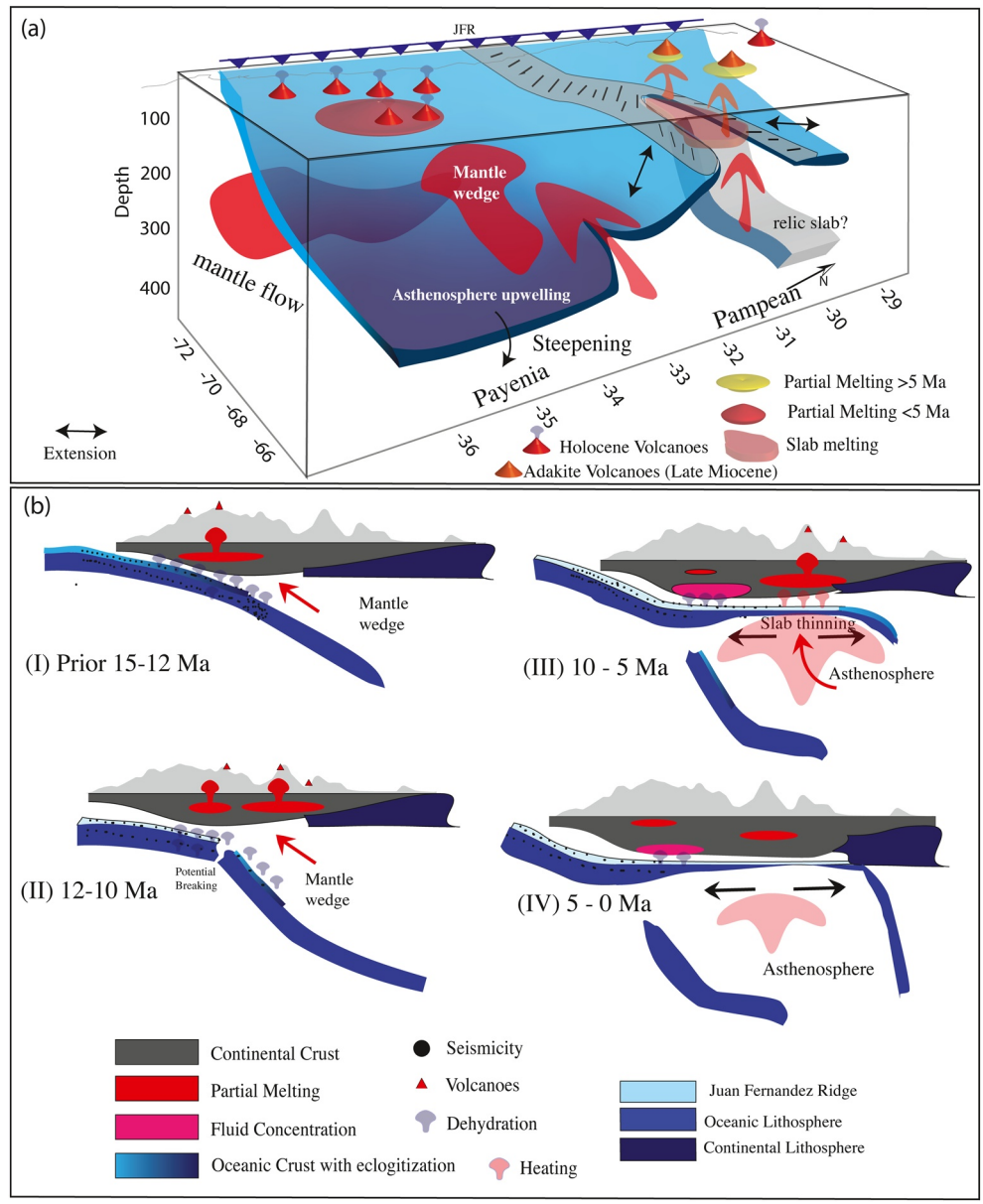

Figure 4. (a) Schematic representation of the current Nazca slab configuration west of 66°W. Gray zone with short bars indicates the inland projection of the Juan Fernandez Ridge. South of 33°S the Nazca plate subducts steeply in the Payenia segment. (b) Proposed sequence of the steep to flat slab subduction evolution along 29°S since 12 Ma, which can explain the observed pattern of Pampean sub-slab anomalies.

faults, causing vigorous intra-slab seismicity (Ammirati et al., 2015; Anderson et al., 2007; Gans et al., 2011; Ranero et al., 2005; Wagner et al., 2020).

Along 30°S, Heit et al. (2008) detected a strong oceanic LAB signal west of 69°W that suddenly disappears and even changes polarity further east below the slab tearing zone (Figure 3b). Recent magnetic and gravity modeling work (Sánchez et al., 2019) also inferred hot asthenospheric flow beneath the flat slab and local slab thinning. These observations support our interpretation of M1 and M2 as evidence for thinning and tearing of the slab (Figure 4).

M1 and M2 are spatially associated with weak crustal low-velocity anomalies C3 and C2 below the late Miocene adakitic volcanism including the GIC (D'Annunzio et al., 2018) and FMG (Kay & Mpodozis, 2002), respectively (Figure 2a). As adakitic volcanism is attributed to melting of the oceanic slab (Gutscher

et al., 2000; Hu & Liu, 2016; Kay & Mpodozis, 2002), which would be expected at the onset of thinning and tearing when the flat slab was being heated up. This indicates a slab tearing at this position might have initiated in the late Miocene during the flattening process and since then started propagating trench-wards (Hu & Liu, 2016) until now, as new slab material is brought into the tearing zone by the ongoing subduction (Figure 4a).

The Pampean flat slab, after having developed in the Middle to Late Miocene, suffered from numerous instabilities, such as internal stresses induced by the increased buoyancy of the JFR relative to its two flanks, changes in hydration state, reactivation of inherited normal faults, and basal heating by asthenosphere flow (Rodríguez-González et al., 2014). These factors have induced weakening, thinning and finally tearing of the oceanic slab, accompanied by melting of the oceanic crust as predicted by the geodynamic model (Hu & Liu, 2016). The basalt input from the melted oceanic crust leads to the adakitic volcanism (Gutscher et al., 2000) during the late Miocene (Figure 4a). However, as Hu and Liu (2016) pointed out, the cessation of adakitic eruption possibly correlated with the waning asthenosphere upwelling after thermal equilibration has been achieved following upward flow of hot asthenospheric material through the gap and cooling-down and even complete closure of the mantle wedge due to the further flattening process after late Miocene (5–3 Ma; Figure 4).

3.3. Slab Break-Off: Transition From Steep to Flat Subduction?

A prominent high-velocity anomaly (H3) is found just below the flat Nazca slab (H2), extending from 28° to 30° (Figure 2d). At depth, H3 is dipping steeply to the east from 200 down to 350 km depth (Profile [a], Figure 3). This anomaly was also visible in previous global or teleseismic tomography studies, but was so far not interpreted (e.g., Li et al., 2008; Mohammadzaheri et al., 2021; Portner et al., 2020). Recent S-wave teleseismic work (Rodríguez et al., 2021) captured a similar but larger-scale high-velocity anomaly extending from 200 km down to the lower mantle and attributed it to a part of relic Phoenix/Aluk plate, which was completely subducted by the late Cretaceous (Gianni et al., 2018; Horton, 2018). However, the resolution of the aforementioned models is limited in the upper mantle due to vertical smearing. We prefer to relate this anomaly to the more recent Nazca plate subduction as it seems unlikely that a part of the Phoenix slab could remain in the upper mantle for more than 100 million years without sinking into the lower mantle or thermally equilibrating with the surrounding mantle (Bello-González et al., 2018; Chen et al., 2019; Ramos & Folguera, 2009). Thus, we propose this anomaly to be a fossil fragment of the Nazca slab that was subducting steeply prior to the onset of flattening, indicating break-off from the leading edge of the current Nazca slab (Liu & Currie, 2016). Slab break-off during the slab flattening process is common in geodynamic models (e.g., Dai et al., 2020; Haschke et al., 2002; Liu & Currie, 2016, 2019). The conditions for slab break-off during the slab flattening process include fast trenchward migration of the overriding plate (high convergence rate) and a strong buoyancy contrast between either an oceanic plateau or aseismic ridge crust (here the JFR) and the normal thickness oceanic crust of an old slab (Haschke et al., 2002; Li et al., 2011; Liu & Currie, 2016, 2019). The removal of the leading dense portion would allow the positive buoyancy of the trailing edge to quickly flatten out the slab (Figure 4b). In many global tomography models, the Nazca slab extends to much shallower depth in the south than the north, where it is visible down to 1,000 km depth (Li et al., 2008; Obayashi et al., 2013). Several teleseismic tomography models (Portner et al., 2017, 2020; Rodríguez et al., 2021) for South America seem to indicate a slab hole at 200–300 km depth around 32°S in the re-steepened portion within the upper mantle. Thus the relic slab break-off or detachment from the head of the young and buoyant Nazca slab seems a viable option.

Taking account of the initial time of the transition from the steep to the flat subduction around 12 Ma coeval with the subduction of the JFR (Kay & Mpodozis, 2002; Ramos & Folguera, 2009; Yáñez et al., 2001), this would also be the time for the high density portion ahead of the JFR to break off from the leading edge of the young Nazca slab (Figure 4b). Furthermore, partial eclogitization of the oceanic crust before the onset of the flat subduction may play an important role in controlling the breaking-off time (Liu & Currie, 2019) and sinking depth in the upper mantle. Thus, the tail of the broken portion would sink slowly in the upper mantle due to its relatively young age, while the head would have already sunk into the mantle transition zone or deeper, below the resolution limit of our model. After break-off, the young and buoyant Nazca slab

with the JFR could lift to extend horizontally eastwards for nearly 300 km before re-steepening with a steep angle to a relatively shallower depth compared to the dip subduction zone north of 28°S (Figure 4b).

We note that the position of the relic slab is further westward than we expected from the geodynamic model of Liu and Currie (2019). While we cannot offer a fully satisfactory explanation for this, we speculate that westward directed asthenospheric flow could potentially account for this discrepancy. In order to solve this puzzle, 3D geodynamic models and future imaging extending high resolution imaging throughout the transition zone and into the uppermost part of the lower mantle will likely be required.

3.4. Subslab Asthenospheric Flow Induced by Sudden Re-Steepening of the Nazca Slab Beneath the Payenia?

Another striking feature in our model is the low-velocity anomaly M4 extending from 32°–36°S below the steep Nazca slab in Payenia subduction zone and from slab depths to 250–300 km depth (Figures 2c and 3, Profile [e]–[h]). This low-velocity anomaly has also been observed by some earlier tomography studies (Celli et al., 2020; Feng et al., 2007; Portner et al., 2017, 2020; Rodríguez et al., 2021). Portner et al. (2017) attributed it to the asthenosphere entrainment by the JFR with the subducting Nazca slab due to the coupling between the asthenosphere and overlying oceanic lithosphere (Liu & Zhou, 2015). However, due to its large size and location, it may more likely be caused by hot asthenospheric flow induced by the sudden re-steepening of the Nazca slab and trench retreat (Hu et al., 2017; Lin, 2014; Mohammadzaheri et al., 2021; Ramos & Folguera, 2009) since 4 Ma beneath the Payenia subduction zone (Figure 4a).

4. Conclusions

Through multi-scale full seismic waveform inversion, we identify low velocity zones within the Pampean flat slab parallel to the inland projection of the Juan Fernandez Ridge, which we interpret as a tearing zone within the flat slab. It may be induced by the buoyancy contrast between the Pampean flat slab with Juan Fernandez Ridge attached and its surrounding steep slab portions to the north and south. Meanwhile, the buoyancy contrast between the young Nazca slab and the preceding steep Nazca slab appears to have triggered the slab break-off from the leading edge of current Nazca slab. The resulting buoyancy increase could possibly sustain the long-distance flat subduction. Flat subduction also expelled the mantle wedge and shut off partial melting, resulting in much reduced volcanic activity and presence of partial melt in the crust. Re-steepening of the Nazca slab beneath the Payenia subduction zone seems to have significantly perturbed the sub-slab asthenospheric flow and introduced large-scale mantle flow, as visible in large low-velocity zone both below and above the slab. Re-opening of the mantle wedge and injection of the asthenosphere induced by the re-steepening of the Nazca slab may have caused the re-accumulation of partial melts within the middle crust and volcanic arc trench-ward migration and reactivation in the Payenia segment.

Data Availability Statement

Waveform data and station meta data were downloaded using the ObsPy (Krischer et al., 2015) module through the International Federation of Digital Seismograph Networks (FDSN) webservices from GEOFON Data Management Center (https://geofon.gfz-potsdam.de/waveform/archive/) and Incorporated Research Institutions for Seismology Data Management Center (IRIS-DMC, http://www.iris.edu/ds/nodes/dmc/). Raw data of the temporary and permanent networks used in this study with FDSN codes including C (https://www.fdsn.org/networks/detail/C/); C1 (https://doi.org/10.7914/SN/C1); CX (https://doi.org/10.14470/PK615318); IU (https://doi.org/10.7914/SN/IU); WA (https://www.fdsn.org/networks/detail/WA/); 2B (https://doi.org/10.14470/7O092361); 3A (https://www.fdsn.org/networks/detail/3A_2010/); 3H (https://doi.org/10.14470/8U7569253520); G (https://doi.org/10.18715/GEOSCOPE.G); X6 (https://doi.org/10.7914/SN/X6_2007); XH (https://doi.org/10.7914/SN/XH_2008); XS (https://doi.org/10.15778/RESIF.XS2010); XY (https://doi.org/10.7914/SN/XY_2010); YC (https://doi.org/10.7914/SN/YC_2000); YM (https://doi.org/10.7914/SN/YM_2010); ZA (https://doi.org/10.14470/MN7557778612); ZB (https://doi.org/10.14470/MO6442843258); ZE (https://geofon.gfz-potsdam.de/waveform/archive/network.php?ncode=ZE&year=2010); ZL (https://doi.org/10.7914/SN/ZL_2007); ZP (https://geofon.gfz-potsdam.de/waveform/archive/network.php?ncode=ZP&year=1999); ZQ (https://geofon.gfz-potsdam.de/waveform/

archive/network.php?ncode=ZQ&year=2004); ZR (https://doi.org/10.7914/SN/ZR_2015); ZW (https://doi.org/10.14470/MJ7559637482). The final velocity model could be accessed through https://doi.org/10.5880/GFZ.2.4.2021.008 (Gao & Tilmann, 2021).

Acknowledgments
The authors gratefully acknowledge fruitful discussions with L. S. Wagner, J. Hu, L. Liu, X. Liu, G. Li, W. Li, T. Zhang, and Y. Yu. The authors thank editor D. Sun, reviewer C. Tape, and one anonymous reviewer for their professional suggestions on the improvement of this manuscript. This work was supported by the Swiss National Supercomputing Center (CSCS) in the form of computing time grants s868 and s1040. Y. Gao is sponsored by Freie Universität Berlin—China Scholarship Council Programm. D.-P. van Herwaarden and S. Thrastarson were supported by the European Research Council (ERC) under the EU's Horizon 2020 program (grant No. 714069). Open access funding enabled and organized by Projekt DEAL.

References

Afanasiev, M., Boehm, C., van Driel, M., Krischer, L., Rietmann, M., May, D. A., et al. (2019). Modular and flexible spectral-element waveform modelling in two and three dimensions. *Geophysical Journal International*, *216*(3), 1675–1692. https://doi.org/10.1093/gji/ggy469

Amante, C., & Eakins, B. W. (2009). *ETOPO1 global relief model converted to PanMap layer format*. PANGAEA. https://doi.org/10.1594/PANGAEA.769615

Ammirati, J.-B., Alvarado, P., & Beck, S. L. (2015). A lithospheric velocity model for the flat slab region of Argentina from joint inversion of Rayleigh wave phase velocity dispersion and teleseismic receiver functions. *Geophysical Journal International*, *202*(1), 224–241. https://doi.org/10.1093/gji/ggv140

Anderson, M., Alvarado, P., Zandt, G., & Beck, S. L. (2007). Geometry and brittle deformation of the subducting Nazca Plate, Central Chile and Argentina. *Geophysical Journal International*, *171*(1), 419–434. https://doi.org/10.1111/j.1365-246x.2007.03483.x

Antonijevic, S. K., Wagner, L. S., Kumar, A., Beck, S. L., Long, M. D., Zandt, G., et al. (2015). The role of ridges in the formation and longevity of flat slabs. *Nature*, *524*(7564), 212–215. https://doi.org/10.1038/nature14648

Axen, G. J., van Wijk, J. W., & Currie, C. A. (2018). Basal continental mantle lithosphere displaced by flat-slab subduction. *Nature Geoscience*, *11*(12), 961–964. https://doi.org/10.1038/s41561-018-0263-9

Beck, S. L., Zandt, G., Ward, K. M., & Scire, A. (2015). Multiple styles and scales of lithospheric foundering beneath the Puna Plateau, central Andes. In P. G. DeCelles, M. N. Ducea, B. Carrapa, & P. A. Kapp (Eds.), *Geodynamics of a cordilleran orogenic system: The central Andes of Argentina and northern Chile*. Geological Society of America. https://doi.org/10.1130/2015.1212(03)

Bello-González, J. P., Contreras-Reyes, E., & Arriagada, C. (2018). Predicted path for hotspot tracks off South America since Paleocene times: Tectonic implications of ridge-trench collision along the Andean margin. *Gondwana Research*, *64*, 216–234. https://doi.org/10.1016/j.gr.2018.07.008

Burd, A. I., Booker, J. R., Mackie, R., Favetto, A., & Pomposiello, M. C. (2014). Three-dimensional electrical conductivity in the mantle beneath the Payún Matrú volcanic field in the Andean backarc of Argentina near 36.5°S: Evidence for decapitation of a mantle plume by resurgent upper mantle shear during slab steepening. *Geophysical Journal International*, *198*(2), 812–827. https://doi.org/10.1093/gji/ggu145

Burd, A. I., Booker, J. R., Mackie, R., Pomposiello, M. C., & Favetto, A. (2013). Electrical conductivity of the Pampean shallow subduction region of Argentina near 33°S: Evidence for a slab window. *Geochemistry, Geophysics, Geosystems*, *14*(8), 3192–3209. https://doi.org/10.1002/ggge.20213

Celli, N. L., Lebedev, S., Schaeffer, A. J., Ravenna, M., & Gaina, C. (2020). The upper mantle beneath the South Atlantic Ocean, South America and Africa from waveform tomography with massive data sets. *Geophysical Journal International*, *221*(1), 178–204. https://doi.org/10.1093/gji/ggz574

Chen, Y. W., Wu, J., & Suppe, J. (2019). Southward propagation of Nazca subduction along the Andes. *Nature*, *565*(7740), 441–447. https://doi.org/10.1038/s41586-018-0860-1

Cristallini, E. O., & Ramos, V. A. (2000). Thick-skinned and thin-skinned thrusting in the La Ramada fold and thrust belt: Crustal evolution of the High Andes of San Juan, Argentina (32°SL). *Tectonophysics*, *317*(3–4), 205–235. https://doi.org/10.1016/s0040-1951(99)00276-0

Dai, L., Wang, L., Lou, D., Li, Z.-H., Dong, H., Ma, F., et al. (2020). Slab rollback versus delamination: Contrasting fates of flat-slab subduction and implications for South China evolution in the Mesozoic. *Journal of Geophysical Research: Solid Earth*, *125*(4), e2019JB019164. https://doi.org/10.1029/2019JB019164

D´Annunzio, M. C., Rubinstein, N., & Rabbia, O. (2018). Petrogenesis of the Gualcamayo Igneous Complex: Regional implications of Miocene magmatism in the Precordillera over the Pampean flat-slab segment, Argentina. *Journal of South American Earth Sciences*, *88*, 16–28. https://doi.org/10.1016/j.jsames.2018.06.012

Ekström, G., Nettles, M., & Dziewoński, A. M. (2012). The global CMT project 2004–2010: Centroid-moment tensors for 13,017 earthquakes. *Physics of the Earth and Planetary Interiors*, *200–201*, 1–9. https://doi.org/10.1016/j.pepi.2012.04.002

Engdahl, E. R., Di Giacomo, D., Sakarya, B., Gkarlaouni, C. G., Harris, J., & Storchak, D. A. (2020). ISC-EHB 1964–2016, an improved data set for studies of earth structure and global seismicity. *Earth and Space Science*, *7*(1), e2019EA000897. https://doi.org/10.1029/2019EA000897

Feng, M., Van der Lee, S., & Assumpção, M. (2007). Upper mantle structure of South America from joint inversion of waveforms and fundamental mode group velocities of Rayleigh waves. *Journal of Geophysical Research*, *112*(B4). https://doi.org/10.1029/2006JB004449

Fichtner, A., Kennett, B. L., Igel, H., & Bunge, H.-P. (2010). Full waveform tomography for radially anisotropic structure: New insights into present and past states of the Australasian upper mantle. *Earth and Planetary Science Letters*, *290*(3–4), 270–280. https://doi.org/10.1016/j.epsl.2009.12.003

Fichtner, A., & Trampert, J. (2011). Resolution analysis in full waveform inversion. *Geophysical Journal International*, *187*(3), 1604–1624. https://doi.org/10.1111/j.1365-246X.2011.05218.x

Folguera, A., Bottesi, G., Zapata, T., & Ramos, V. A. (2008). Crustal collapse in the Andean backarc since 2 Ma: Tromen volcanic plateau, Southern Central Andes (36°40′–37°30′S). *Tectonophysics*, *459*(1–4), 140–160. https://doi.org/10.1016/j.tecto.2007.12.013

Gans, C. R., Beck, S. L., Zandt, G., Gilbert, H., Alvarado, P., Anderson, M., & Linkimer, L. (2011). Continental and oceanic crustal structure of the Pampean flat slab region, western Argentina, using receiver function analysis: New high-resolution results. *Geophysical Journal International*, *186*(1), 45–58. https://doi.org/10.1111/j.1365-246X.2011.05023.x

Gao, Y., & Tilmann, F. (2021). Seismic velocity model of crust and upper mantle beneath South Central Andes including Pampean and Payenia [Data set]. *GFZ Data Services*, Potsdam, Germany. https://doi.org/10.5880/GFZ.2.4.2021.008

Gao, Y., Tilmann, F., van Herwaarden, D.-P., Thrastarson, S., Fichtner, A., Heit, B., et al. (2021). Full waveform inversion beneath the Central Andes: Insight into the dehydration of the Nazca slab and delamination of the back-arc lithosphere. *Journal of Geophysical Research: Solid Earth*, *126*(7), e2021JB021984. https://doi.org/10.1029/2021JB021984

Gianni, G., Pesce, A., & Soler, S. (2018). Transient plate contraction between two simultaneous slab windows: Insights from Paleogene tectonics of the Patagonian Andes. *Journal of Geodynamics*, *121*, 64–75. https://doi.org/10.1016/j.jog.2018.07.008

Goss, A. R., Kay, S. M., Mpodozis, C., & Singer, B. S. (2009). The Incapillo Caldera and Dome Complex (~28° S, Central Andes): A stranded magma chamber over a dying arc. *Journal of Volcanology and Geothermal Research*, *184*(3–4), 389–404. https://doi.org/10.1016/j.jvolgeores.2009.05.005

Goss, A. R., Kay, S. M., & Mpodozis, C. (2011). The geochemistry of a dying continental arc: The Incapillo Caldera and Dome Complex of the southernmost Central Andean Volcanic Zone (~28°S). *Contributions to Mineralogy and Petrology*, *161*(1), 101–128. https://doi.org/10.1007/s00410-010-0523-1

Gutscher, M.-A., Maury, R., Eissen, J.-P., & Bourdon, E. (2000). Can slab melting be caused by flat subduction? *Geology*, *28*(6), 535–538. https://doi.org/10.1130/0091-7613(2000)028<0535:csmbcb>2.3.co;2

Haddon, A., & Porter, R. (2018). S-wave receiver function analysis of the Pampean Flat-Slab Region: Evidence for a Torn Slab. *Geochemistry, Geophysics, Geosystems*, *19*(10), 4021–4034. https://doi.org/10.1029/2018GC007868

Haschke, M., Scheuber, E., Günther, A., & Reutter, K.-J. (2002). Evolutionary cycles during the Andean orogeny: Repeated slab breakoff and flat subduction? *Terra Nova*, *14*(1), 49–55. https://doi.org/10.1046/j.1365-3121.2002.00387.x

Hayes, G. P., Moore, G. L., Portner, D. E., Hearne, M., Flamme, H., Furtney, M., & Smoczyk, G. M. (2018). Slab2, a comprehensive subduction zone geometry model. *Science*, *362*(6410), 58–61. https://doi.org/10.1126/science.aat4723

Heit, B., Yuan, X., Bianchi, M., Sodoudi, F., & Kind, R. (2008). Crustal thickness estimation beneath the southern central Andes at 30°S and 36°S from S wave receiver function analysis. *Geophysical Journal International*, *174*(1), 249–254. https://doi.org/10.1111/j.1365-246x.2008.03780.x

Hiett, C. D., Newell, D. L., & Jessup, M. J. (2021). ^{3}He evidence for fluid transfer and continental hydration above a flat slab. *Earth and Planetary Science Letters*, *556*, 116722. https://doi.org/10.1016/j.epsl.2020.116722

Hildreth, W., & Moorbath, S. (1988). Crustal contributions to arc magmatism in the Andes of central Chile. *Contributions to Mineralogy and Petrology*, *98*(4), 455–489. https://doi.org/10.1007/BF00372365

Horton, B. K. (2018). Tectonic regimes of the central and southern Andes: Responses to variations in plate coupling during subduction. *Tectonics*, *37*(2), 402–429. https://doi.org/10.1002/2017TC004624

Hu, J., Faccenda, M., & Liu, L. (2017). Subduction-controlled mantle flow and seismic anisotropy in South America. *Earth and Planetary Science Letters*, *470*, 13–24. https://doi.org/10.1016/j.epsl.2017.04.027

Hu, J., & Liu, L. (2016). Abnormal seismological and magmatic processes controlled by the tearing South American flat slabs. *Earth and Planetary Science Letters*, *450*, 40–51. https://doi.org/10.1016/j.epsl.2016.06.019

Kay, R. W., & Kay, S. M. (2002). Andean adakites: Three ways to make them. *Acta Petrologica Sinica*, *18*(3), 303–311.

Kay, S. M., & Abbruzzi, J. M. (1996). Magmatic evidence for Neogene lithospheric evolution of the central Andean "flat-slab" between 30°S and 32°S. *Tectonophysics*, *259*(1–3), 15–28. https://doi.org/10.1016/0040-1951(96)00032-7

Kay, S. M., & Coira, B. L. (2009). Shallowing and steepening subduction zones, continental lithospheric loss, magmatism, and crustal flow under the Central Andean Altiplano-Puna Plateau. *Backbone of the Americas: Shallow Subduction, Plateau Uplift, and Ridge and Terrane Collision*, *204*, 229. https://doi.org/10.1130/2009.1204(11)

Kay, S. M., Godoy, E., & Kurtz, A. (2005). Episodic arc migration, crustal thickening, subduction erosion, and magmatism in the south-central Andes. *Geological Society of America Bulletin*, *117*(1), 67. https://doi.org/10.1130/b25431.1

Kay, S. M., & Mpodozis, C. (2002). Magmatism as a probe to the Neogene shallowing of the Nazca plate beneath the modern Chilean flat-slab. *Journal of South American Earth Sciences*, *15*(1), 39–57. https://doi.org/10.1016/S0895-9811(02)00005-6

Kendrick, E., Bevis, M., Smalley, R., Jr., Brooks, B., Vargas, R. B., Lauria, E., & Fortes, L. P. S. (2003). The Nazca-South America Euler vector and its rate of change. *Journal of South American Earth Sciences*, *16*(2), 125–131. https://doi.org/10.1016/S0895-9811(03)00028-2

Koelemeijer, P., Ritsema, J., Deuss, A., & van Heijst, H.-J. (2015). SP12RTS: A degree-12 model of shear- and compressional-wave velocity for Earth's mantle. *Geophysical Journal International*, *204*(2), 1024–1039. https://doi.org/10.1093/gji/ggv481

Kopp, H., Flueh, E. R., Papenberg, C., & Klaeschen, D. (2004). Seismic investigations of the O'Higgins Seamount Group and Juan Fernández Ridge: Aseismic ridge emplacement and lithosphere hydration. *Tectonics*, *23*(2). https://doi.org/10.1029/2003TC001590

Krischer, L., Megies, T., Barsch, R., Beyreuther, M., Lecocq, T., Caudron, C., & Wassermann, J. (2015). ObsPy: A bridge for seismology into the scientific python ecosystem. *Computational Science & Discovery*, *8*(1), 014003. https://doi.org/10.1088/1749-4699/8/1/014003

Li, C., Van Der Hilst, R. D., Engdahl, E. R., & Burdick, S. (2008). A new global model for P wave speed variations in Earth's mantle. *Geochemistry, Geophysics, Geosystems*, *9*(5). https://doi.org/10.1029/2007GC001806

Li, Z. (2020). Flat subduction versus big mantle wedge: Contrasting modes for deep hydration and overriding craton modification. *Journal of Geophysical Research: Solid Earth*, *125*(8). https://doi.org/10.1029/2020JB020018

Li, Z., Xu, Z., & Gerya, T. (2011). Flat versus steep subduction: Contrasting modes for the formation and exhumation of high-to ultra-high-pressure rocks in continental collision zones. *Earth and Planetary Science Letters*, *301*(1–2), 65–77. https://doi.org/10.1016/j.epsl.2010.10.014

Lin, S. (2014). Three-dimensional mantle circulations and lateral slab deformation in the southern Chilean subduction zone. *Journal of Geophysical Research: Solid Earth*, *119*(4), 3879–3896. https://doi.org/10.1002/2013JB010864

Linkimer, L., Beck, S., Zandt, G., Alvarado, P., Anderson, M., Gilbert, H., & Zhang, H. (2020). Lithospheric structure of the Pampean flat slab region from double-difference tomography. *Journal of South American Earth Sciences*, *97*, 102417. https://doi.org/10.1016/j.jsames.2019.102417

Liu, L., & Zhou, Q. (2015). Deep recycling of oceanic asthenosphere material during subduction. *Geophysical Research Letters*, *42*(7), 2204–2211. https://doi.org/10.1002/2015GL063633

Liu, S., & Currie, C. A. (2016). Farallon plate dynamics prior to the Laramide orogeny: Numerical models of flat subduction. *Tectonophysics*, *666*, 33–47. https://doi.org/10.1016/j.tecto.2015.10.010

Liu, X., & Currie, C. A. (2019). Influence of upper plate structure on flat-slab depth: Numerical modeling of subduction dynamics. *Journal of Geophysical Research: Solid Earth*, *124*(12), 13150–13167. https://doi.org/10.1029/2019JB018653

Lynner, C., Anderson, M. L., Portner, D. E., Beck, S. L., & Gilbert, H. (2017). Mantle flow through a tear in the Nazca slab inferred from shear wave splitting. *Geophysical Research Letters*, *44*(13), 6735–6742. https://doi.org/10.1002/2017GL074312

Manea, V. C., Manea, M., Ferrari, L., Orozco-Esquivel, T., Valenzuela, R., Husker, A., & Kostoglodov, V. (2017). A review of the geodynamic evolution of flat slab subduction in Mexico, Peru, and Chile. *Tectonophysics*, *695*, 27–52. https://doi.org/10.1016/j.tecto.2016.11.037

Manea, V. C., Pérez-Gussinyé, M., & Manea, M. (2012). Chilean flat slab subduction controlled by overriding plate thickness and trench rollback. *Geology*, *40*(1), 35–38. https://doi.org/10.1130/G32543.1

Marot, M., Monfret, T., Gerbault, M., Nolet, G., Ranalli, G., & Pardo, M. (2014). Flat versus normal subduction zones: A comparison based on 3-D regional traveltime tomography and petrological modelling of central Chile and western Argentina (29°–35°S). *Geophysical Journal International*, *199*(3), 1633–1654. https://doi.org/10.1093/gji/ggu355

Mohammadzaheri, A., Sigloch, K., Hosseini, K., & Mihalynuk, M. G. (2021). Subducted lithosphere under South America from multifrequency P wave tomography. *Journal of Geophysical Research: Solid Earth*, *126*(6), e2020JB020704. https://doi.org/10.1029/2020JB020704
Obayashi, M., Yoshimitsu, J., Nolet, G., Fukao, Y., Shiobara, H., Sugioka, H., et al. (2013). Finite frequency whole mantle P wave tomography: Improvement of subducted slab images. *Geophysical Research Letters*, *40*(21), 5652–5657. https://doi.org/10.1002/2013gl057401
Pesicek, J. D., Engdahl, E. R., Thurber, C. H., DeShon, H. R., & Lange, D. (2012). Mantle subducting slab structure in the region of the 2010 M8.8 Maule earthquake (30-40°S), Chile. *Geophysical Journal International*, *191*(1), 317–324. https://doi.org/10.1111/j.1365-246x.2012.05624.x
Piceda, C. R., Wenderoth, M. S., Dacal, M. L. G., Bott, J., Prezzi, C. B., & Strecker, M. R. (2020). Lithospheric density structure of the Southern Central Andes constrained by 3D data-integrative gravity modelling. *International Journal of Earth Sciences*, *110*, 2333–2359. https://doi.org/10.1007/s00531-020-01962-1
Porter, R., Gilbert, H., Zandt, G., Beck, S., Warren, L., Calkins, J., et al. (2012). Shear wave velocities in the Pampean flat-slab region from Rayleigh wave tomography: Implications for slab and upper mantle hydration. *Journal of Geophysical Research: Solid Earth*, *117*(11). https://doi.org/10.1029/2012JB009350
Portner, D. E., Beck, S., Zandt, G., & Scire, A. (2017). The nature of subslab slow velocity anomalies beneath South America. *Geophysical Research Letters*, *44*(10), 4747–4755. https://doi.org/10.1002/2017GL073106
Portner, D. E., Rodríguez, E. E., Beck, S. L., Zandt, G., Scire, A., Rocha, M. P., et al. (2020). Detailed structure of the subducted Nazca slab into the lower mantle derived from continent-scale teleseismic P Wave tomography. *Journal of Geophysical Research: Solid Earth*, *125*(5). https://doi.org/10.1029/2019JB017884
Ramos, V. A., Cristallini, E. O., & Pérez, D. J. (2002). The Pampean flat-slab of the central Andes. *Journal of South American Earth Sciences*, *15*(1), 59–78. https://doi.org/10.1016/S0895-9811(02)00006-8
Ramos, V. A., & Folguera, A. (2009). Andean flat-slab subduction through time. *Geological Society, London, Special Publications*, *327*(1), 31–54. https://doi.org/10.1144/SP327.3
Ramos, V. A., & Folguera, A. (2011). Payenia volcanic province in the southern Andes: An appraisal of an exceptional quaternary tectonic setting. *Journal of Volcanology and Geothermal Research*, *201*(1–4), 53–64. https://doi.org/10.1016/j.jvolgeores.2010.09.008
Ramos, V. A., Litvak, V. D., Folguera, A., & Spagnuolo, M. (2014). An Andean tectonic cycle: From crustal thickening to extension in a thin crust (34–37 SL). *Geoscience Frontiers*, *5*(3), 351–367. https://doi.org/10.1016/j.gsf.2013.12.009
Ranero, C. R., Villaseñor, A., Phipps Morgan, J., & Weinrebe, W. (2005). Relationship between bend-faulting at trenches and intermediate-depth seismicity. *Geochemistry, Geophysics, Geosystems*, *6*(12). https://doi.org/10.1029/2005GC000997
Rivadeneyra-Vera, C., Bianchi, M., Assumpção, M., Cedraz, V., Julià, J., Rodríguez, M., et al. (2019). An updated crustal thickness map of central South America based on receiver function measurements in the region of the Chaco, Pantanal, and Paraná Basins, southwestern Brazil. *Journal of Geophysical Research: Solid Earth*, *124*(8), 8491–8505. https://doi.org/10.1029/2018JB016811
Rodríguez, E. E., Portner, D. E., Beck, S. L., Rocha, M. P., Bianchi, M. B., Assumpção, M., et al. (2021). Mantle dynamics of the Andean Subduction Zone from continent-scale teleseismic S-wave tomography. *Geophysical Journal International*, *224*(3), 1553–1571. https://doi.org/10.1093/gji/ggaa536
Rodríguez-González, J., Negredo, A. M., & Carminati, E. (2014). Slab-mantle flow interaction: Influence on subduction dynamics and duration. *Terra Nova*, *26*(4), 265–272. https://doi.org/10.1111/ter.12095
Sánchez, M. A., García, H. P., Acosta, G., Gianni, G. M., Gonzalez, M. A., Ariza, J. P., et al. (2019). Thermal and lithospheric structure of the Chilean-Pampean flat-slab from gravity and magnetic data. In *Andean tectonics* (pp. 487–507). Elsevier. https://doi.org/10.1016/B978-0-12-816009-1.00005-8
Sippl, C., Moreno, M. & Benavente, R. (2021). Microseismicity appears to outline highly coupled regions on the Central Chile megathrust. *Journal of Geophysical Research: Solid Earth*, *126*, e2021JB022252. https://doi.org/10.1029/2021JB022252
Spagnuolo, M. G., Litvak, V. D., Folguera, A., Bottesi, G., & Ramos, V. A. (2012). Neogene magmatic expansion and mountain building processes in the southern Central Andes, 36–37°S, Argentina. *Journal of Geodynamics*, *53*, 81–94. https://doi.org/10.1016/j.jog.2011.07.004
Tao, K., Grand, S. P., & Niu, F. (2018). Seismic structure of the upper mantle beneath eastern Asia from full waveform seismic tomography. *Geochemistry, Geophysics, Geosystems*, *19*(8), 2732–2763. https://doi.org/10.1029/2018GC007460
Tape, C., Liu, Q., Maggi, A., & Tromp, J. (2010). Seismic tomography of the southern California crust based on spectral-element and adjoint methods. *Geophysical Journal International*, *180*(1), 433–462. https://doi.org/10.1111/j.1365-246X.2009.04429.x
Tassara, A., Götze, H.-J., Schmidt, S., & Hackney, R. (2006). Three-dimensional density model of the Nazca plate and the Andean continental margin. *Journal of Geophysical Research*, *111*(B9). https://doi.org/10.1029/2005JB003976
Wagner, L. S., Beck, S. L., & Zandt, G. (2005). Upper mantle structure in the south central Chilean subduction zone (30 to 36°S). *Journal of Geophysical Research*, *110*(B1). https://doi.org/10.1029/2004JB003238
Wagner, L. S., Caddick, M. J., Kumar, A., Beck, S. L., & Long, M. D. (2020). Effects of oceanic crustal thickness on intermediate depth seismicity. *Frontiers in Earth Science*, *8*. https://doi.org/10.3389/feart.2020.00244
Ward, K. M., Delph, J. R., Zandt, G., Beck, S. L., & Ducea, M. N. (2017). Magmatic evolution of a Cordilleran flare-up and its role in the creation of silicic crust. *Scientific Reports*, *7*(1), 1–8. https://doi.org/10.1038/s41598-017-09015-5
Ward, K. M., Porter, R. C., Zandt, G., Beck, S. L., Wagner, L. S., Minaya, E., & Tavera, H. (2013). Ambient noise tomography across the Central Andes. *Geophysical Journal International*, *194*(3), 1559–1573. https://doi.org/10.1093/gji/ggt166
Ward, K. M., Zandt, G., Beck, S. L., Christensen, D. H., & McFarlin, H. (2014). Seismic imaging of the magmatic underpinnings beneath the Altiplano-Puna volcanic complex from the joint inversion of surface wave dispersion and receiver functions. *Earth and Planetary Science Letters*, *404*, 43–53. https://doi.org/10.1016/j.epsl.2014.07.022
Yáñez, G. A., Ranero, C. R., Von Huene, R., & Díaz, J. (2001). Magnetic anomaly interpretation across the southern central Andes (32°–34°S): The role of the Juan Fernández Ridge in the late Tertiary evolution of the margin. *Journal of Geophysical Research*, *106*(B4), 6325–6345. https://doi.org/10.1029/2000jb900337
Yuan, X., Sobolev, S. V., Kind, R., Oncken, O., Bock, G., Asch, G., et al. (2000). Subduction and collision processes in the Central Andes constrained by converted seismic phases. *Nature*, *408*(6815), 958–961. https://doi.org/10.1038/35050073

References From the Supporting Information

Albuquerque Seismological Laboratory (ASL)/USGS. (1988). *Global seismograph network (GSN-IRIS/USGS)*. International Federation of Digital Seismograph Networks. https://doi.org/10.7914/SN/IU

Asch, G., Heit, B., & Yuan, X. (2002). *The ReFuCA project: Receiver functions central Andes*. Deutsches GeoForschungsZentrum GFZ. https://doi.org/10.14470/MN7557778612

Beck, S. L., Wallace, T., & Zandt, G. (2000). *Slab geometry in the Southern Andes*. International Federation of Digital Seismograph Networks. https://doi.org/10.7914/SN/YC_2000

Beck, S. L., & Zandt, G. (2007). *Lithospheric structure and deformation of the flat slab region of Argentina*. International Federation of Digital Seismograph Networks. https://doi.org/10.7914/SN/ZL_2007

Dziewonski, A. M., & Anderson, D. L. (1981). Preliminary reference Earth model. *Physics of the Earth and Planetary Interiors*, *25*(4), 297–356. https://doi.org/10.1016/0031-9201(81)90046-7

Fichtner, A., & Leeuwen, T. V. (2015). Resolution analysis by random probing. *Journal of Geophysical Research: Solid Earth*, *120*(8), 5549–5573. https://doi.org/10.1002/2015JB012106

GFZ, & CNRS-INSU. (2006). *IPOC seismic network*. Integrated Plate Boundary Observatory Chile—IPOC. https://doi.org/10.14470/PK615318

Gilbert, H. (2008). *Eastern Sierras Pampeanas, lithospheric structure above the variably dipping Nazca Slab*. International Federation of Digital Seismograph Networks. https://doi.org/10.7914/SN/XH_2008

Heit, B., Yuan, X., Kind, R., & Asch, G. (2007). *Lithospheric dynamics in the southernmost Andean Plateau (PUDEL)*. Deutsches GeoForschungsZentrum GFZ. https://doi.org/10.14470/7O092361

Hirt, C., & Rexer, M. (2015). Earth2014: 1 arc-min shape, topography, bedrock and ice-sheet models—Available as gridded data and degree-10,800 spherical harmonics. *International Journal of Applied Earth Observation and Geoinformation*, *39*, 103–112. https://doi.org/10.1016/j.jag.2015.03.001

IPGP and EOST. (1982). *GEOSCOPE, French global network of broad band seismic stations*: Institut de physique du globe de Paris (IPGP). https://doi.org/10.18715/GEOSCOPE

Krischer, L., Fichtner, A., Zukauskaite, S., & Igel, H. (2015). Large-scale seismic inversion framework. *Seismological Research Letters*, *86*(4), 1198–1207. https://doi.org/10.1785/0220140248

Lange, D., Cembrano, J., & Sielfeld, G. (2019). *Crustal seismicity along for the southern Andes volcanic zone (LOFS)*. GFZ Data Services. https://doi.org/10.14470/8U7569253520

Laske, G., Masters, G., Ma, Z., & Pasyanos, M. (2013). Update on CRUST1. 0—A 1-degree global model of Earth's crust. *Geophysical Research Abstracts*, *15*–2658.

Liu, D., & Nocedal, J. (1989). On the limited memory BFGS method for large scale optimization. *Mathematical Programming*, *45*(1–3), 503–528. https://doi.org/10.1007/bf01589116

Pavlis, N. K., Holmes, S. A., Kenyon, S. C., & Factor, J. K. (2012). The development and evaluation of the Earth Gravitational Model 2008 (EGM2008). *Journal of Geophysical Research*, *117*(B4). https://doi.org/10.1029/2011JB008916

Rietbrock, A., Haberland, C., Bataille, K., Lange, D., & Dahm, T. (2004). *TIPTEQ-temporary seismological network (North) (2004/2005)*. GFZ Data Services. https://doi.org/10.14470/MJ7559637482

Roecker, S., & Russo, R. (2010). *RAMP response for 2010 earthquake*. International Federation of Digital Seismograph Networks. https://doi.org/10.7914/SN/XY_2010

Sandvol, E., & Brown, L. (2007). *SLIP—seismic lithospheric imaging of the Puna plateau*. International Federation of Digital Seismograph Networks. https://doi.org/10.7914/SN/X6_2007

Schurr, B., Asch, G., & Wigger, P. (1997). *PUNA project*. GFZ Data Services. https://doi.org/10.14470/MO6442843258

Thrastarson, S., van Herwaarden, D. P., Krischer, L., & Fichtner, A. (2021). *LASIF: Large-scale seismic inversion framework*. https://doi.org/10.31223/X5NC84

Thurber, C. (2015). *Laguna del Maule seismic imaging* [Data set]. International Federation of Digital Seismograph Networks. https://doi.org/10.7914/SN/ZR_2015

Universidad De Chile. (2013). *Red Sismologica Nacional*. International Federation of Digital Seismograph Networks. https://doi.org/10.7914/SN/C1

Vilotte, J.-P., & RESIF. (2011). *Seismic network XS: CHILE MAULE aftershock temporary experiment (RESIF-SISMOB)*. RESIF - Réseau Sismologique et géodésique Français. https://doi.org/10.15778/RESIF.XS2010

Waite, G. P. (2010). *An integrated analysis of low-frequency seismicity at Villarrica Volcano, Chile* [Data set]. International Federation of Digital Seismograph Networks. https://doi.org/10.7914/SN/YM_2010

Zhu, H., Bozdağ, E., & Tromp, J. (2015). Seismic structure of the European upper mantle based on adjoint tomography. *Geophysical Journal International*, *201*(1), 18–52. https://doi.org/10.1093/gji/ggu492

Zhu, H., Komatitsch, D., & Tromp, J. (2017). Radial anisotropy of the North American upper mantle based on adjoint tomography with USArray. *Geophysical Journal International*, *211*(1), 349–377. https://doi.org/10.1093/gji/ggx305